Broadband tunable Raman soliton self-frequency shift to mid-infrared band in a highly birefringent microstructure fiber*

Wei Wang(王伟)[1,2,†], Xin-Ying Bi(毕新英)[1,2], Jun-Qi Wang(王珺琪)[1,2], Yu-Wei Qu(屈玉玮)[1,2], Ying Han(韩颖)[1,2], Gui-Yao Zhou(周桂耀)[1,2], and Yue-Feng Qi(齐跃峰)[1,2]

[1] *School of Information Science and Engineering, Yanshan University, Qinhuangdao* 066004, *China*
[2] *The Key Laboratory for Special Fiber and Fiber Sensor of Hebei Province, Qinhuangdao* 066004, *China*

(Received 8 October 2015; revised manuscript received 29 January 2016; published online 1 June 2016)

Raman soliton self-frequency shifted to mid-infrared band ($\lambda > 2$ μm) has been achieved in an air-silica microstructure fiber (MF). The MF used in our experiment has an elliptical core with diameters of 1.08 and 2.48 μm for fast and slow axis. Numerical simulation shows that each fundamental orthogonal polarization mode has two wide-spaced λ_{ZDW} and the λ_{ZDW} pairs located at 701/2110 nm and 755/2498 nm along the fast and slow axis, respectively. Using 810-nm Ti:sapphire femtosecond laser as pump, when the output power varies from 0.3 to 0.5 W, the furthest red-shift Raman solitons in both fast and slow axis shift from near-infrared band to mid-infrared band, reaching as far as 2030 and 2261 nm. Also, mid-infrared Raman solitons can always be generated for pump wavelength longer than 790 nm if output pump power reaches 0.5 W. Specifically, with pump power at 0.5 W, the mid-infrared soliton in slow axis shifts from 2001 to 2261 nm when the pump changes from 790 nm to 810 nm. This means only a 20 nm change of pump results in 260 nm tunability of a mid-infrared soliton.

Keywords: Raman soliton, soliton self-frequency shift, mid-infrared, microstructure fiber

PACS: 42.65.Tg, 42.65.–k, 42.25.Lc, 42.81.–i **DOI:** 10.1088/1674-1056/25/7/074206

1. Introduction

Pulsed-laser sources in mid-infrared (MIR, $\lambda > 2$ μm) bands[1–4] with high peak powers and repetition rates are promising for a broad range of applications, such as IR spectroscopy, biophotonics, polymer chemistry, etc.,[5–7] since many molecular transitions locate in this range. Microstructure fiber (MF) is a kind of optical fiber whose zero dispersion wavelength λ_{ZDW}[8–11] can be wide-band adjusted, even to the visible region. In addition, MF can have very high nonlinear coefficient that is hardly achievable in conventional fiber. The features mentioned above provide a possibility for strong Raman soliton self-frequency shift (SSFS)[12–19] and make MF an ideal medium for high peak power, high repetition, wide-band ultra-short tunable Raman soliton generation.

As early as 2001, a near-infrared femtosecond Raman soliton has been generated in air-silica MF. Washburn *et al.*[13] demonstrated a tunable near-infrared (850–1050 nm) femtosecond Raman soliton by pumping MF with 110-fs pulses. Liu *et al.*[14] reported an SSFS tunable from 1.3 to 1.65 μm with 60% conversion efficiency in a 15-cm tapered MF. In 2009, Masip *et al.*[15] presented a complete set of measurements and numerical simulations of a femtosecond soliton source in an MF with spectral tunability from 850 to 1200 nm. These solitons keep almost a constant time duration of 40 fs and spectral widths of 20 nm over the entire measured spectra regardless of input power. However, it is difficult to shift solitons to MIR in air-silica MF due to relatively short λ_{ZDW} and relatively high loss beyond 2 μm for silica. For SSFS to MIR, exotic materials such as tellurite, chalcogenide, and heavy metal fluoride are used instead of silica for fiber fabrication. In 2014, SSFS with a soliton central wavelength from 2.986 to 3.419 μm is observed when a hybrid four-hole $AsSe_2$-As_2S_5 MF is pumped by an optical parametric oscillator at 2.8 μm.[16]

In this paper, a mid-infrared Raman soliton, reaching as far as 2261 nm, is achieved in a home-made air-silica highly birefringent MF (HB-MF) using Ti-sapphire fs pulse as pump. The red-shift of Raman solitons is investigated for each fundamental orthogonal polarized mode under different pump powers and wavelengths.

2. Theoretical fundamentals

The effective index n_{eff}^x and n_{eff}^y corresponding to two fundamental orthogonal polarization modes of HB-MF are calculated by full vector finite element method with the index of silica setting to 1.45. The modal birefringence $B(\lambda)$ can be calculated by

$$B(\lambda) = \left| n_{\text{eff}}^x - n_{\text{eff}}^y \right|. \tag{1}$$

The waveguide dispersion $D_{\text{w}}^i(\lambda)$ of two fundamental or-

*Project supported by the National Natural Science Foundation of China (Grant Nos. 61405172, 61405173, and 61275093), the Natural Science Foundation of Hebei Province, China (Grant No. F2014203194), the College Science Research Program of Hebei Province, China (Grant No. QN20131044), and the Program of Independent Research for the Young Teachers of Yanshan University of China (Grant No. 13LGB017).

†Corresponding author. E-mail: wangwei@ysu.edu.cn

© 2016 Chinese Physical Society and IOP Publishing Ltd

thogonal modes can be obtained by

$$D^i_{\rm w}(\lambda) = -\frac{\lambda}{c}\frac{{\rm d}^2 n^i_{\rm eff}(\lambda)}{{\rm d}\lambda^2}, \quad i = x \ \text{ or } \ y, \tag{2}$$

where c is the velocity of light in vacuum, and λ is the wavelength of light.

Then, the total dispersion $D^i(\lambda)$ is given by

$$D^i(\lambda) = D^i_{\rm w}(\lambda) + D_{\rm m}(\lambda), \quad i = x \ \text{ or } \ y, \tag{3}$$

which includes the waveguide dispersion $D^i_{\rm w}(\lambda)$ and material dispersion

$$D_{\rm m}(\lambda) = -\frac{\lambda}{c}\frac{{\rm d}^2 n_{\rm silica}(\lambda)}{{\rm d}\lambda^2}.$$

Here, the index of silica $n_{\rm silica}$ is approximated by Sellmeier formula[17]

$$n^2_{\rm silica}(\omega) = 1 + \sum_{j=1}^{m}\frac{B_j\omega_j^2}{\omega_j^2 - \omega^2}, \tag{4}$$

where ω_j is the resonant frequency, and B_j is the resonant intensity.

The effective mode area $A_{\rm eff}$ can be obtained by

$$A_{\rm eff} = \frac{\left(\iint |\boldsymbol{E}^2|{\rm d}x{\rm d}y\right)^2}{\left(\iint |E|^4{\rm d}x{\rm d}y\right)}, \tag{5}$$

where $\boldsymbol{E}$ is the electric field derived by solving the Maxwell equations. Then, the nonlinear coefficient γ can be calculated through

$$\gamma = \frac{2\pi}{\lambda}\frac{n_2}{A_{\rm eff}}, \tag{6}$$

where $n_2 = 2.2\times10^{-20}$ m$^2\cdot$W^{-1} is the nonlinear refractive index of the silica.

3. Results and discussion

The MF used in our experiment is a home-made HB-MF with an elliptical core (see inset of Fig. 1). The diameters of slow and fast axis (or x and y axis) are 2.48 and 1.08 μm, respectively. Due to large air-filling fraction, cladding air holes bear some kind of deformation. To improve computational accuracy, actual fiber structure based on the photo of the MF is introduced in numerical simulation. From Fig. 1, we can see that with wavelength changing from 400 to 2500 nm, $B(\lambda)$ (right y axis) increases from 3.22×10^{-3} to 2.85×10^{-2}, which is nearly 2 orders of magnitude higher than traditional birefringence fiber. Figure 1 also shows the dispersion curves (left y axis) of two fundamental orthogonal polarization modes. Both modes have two wide-spaced $\lambda_{\rm ZDW}$, and the $\lambda_{\rm ZDW}$ pairs are 701/2110 nm and 755/2498 nm along the fast and slow axis, respectively. The output spectrum of Ti:sapphire fs laser is well covered by the anomalous dispersion region. This makes Ti:sapphire laser a suitable source for fs soliton formation.

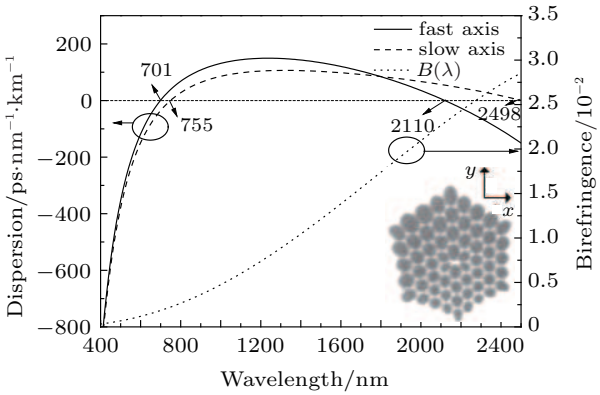


Fig. 1. (color online) Group velocity dispersion and birefringence. The inset shows the cross section of HB-MF.

Figure 2 shows the nonlinear coefficient (left y axis) and the effective mode area (right y axis) of two fundamental orthogonal polarization modes. For the HB-MF used here, the $A_{\rm eff}$ is only 2.17 and 2.25 μm^2 for x and y polarized mode at 800 nm, corresponding to nonlinear coefficient γ as high as 79.70 and 76.75 km$^{-1}\cdot$W^{-1}, respectively. Seen from Fig. 2, the y polarized mode has larger $A_{\rm eff}$ and smaller γ compared with the x polarized mode. The guiding modes of MF are essentially a kind of leaky mode. The diameter of the fast axis is too small to confine the light tightly in the fiber core, and more light would penetrate from core to cladding, which results in larger $A_{\rm eff}$ and smaller γ. It can also be concluded that the loss of y polarized mode is larger than x polarized mode due to poor ability of light confinement. Thus, the slow axis is favored for strong Raman SSFS.

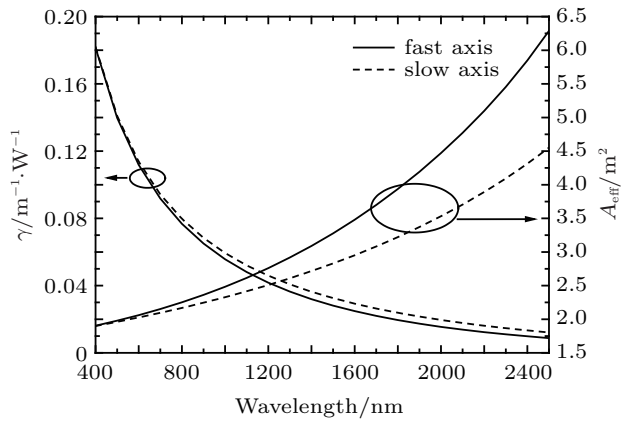


Fig. 2. The effective mode area and nonlinear coefficient.

The experimental setup is shown in Fig. 3. A Ti:sapphire laser (Coherent Mira900) with output pulse of 120 fs and repetition rate of 76 MHz is used as pump. A 1/2 wave plate is employed to adjust the angle between input pump beam and fiber axis. Then, the pump pulse is coupled into 1.15-m HB-MF by a 40× objective lens and output spectra is coupled into a bifurcated fiber to be monitored by two optical spectrum analyzers (Avaspec-256 and Avaspec-NIR-256) simultaneously.

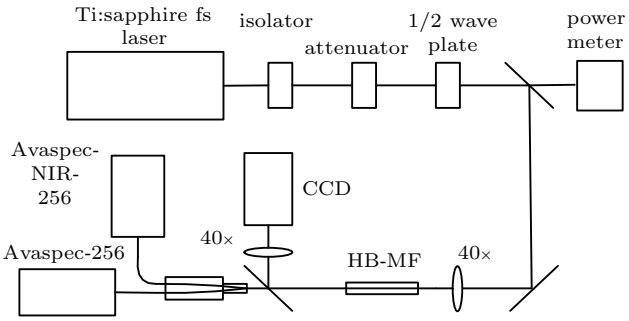


Fig. 3. Experimental setup.

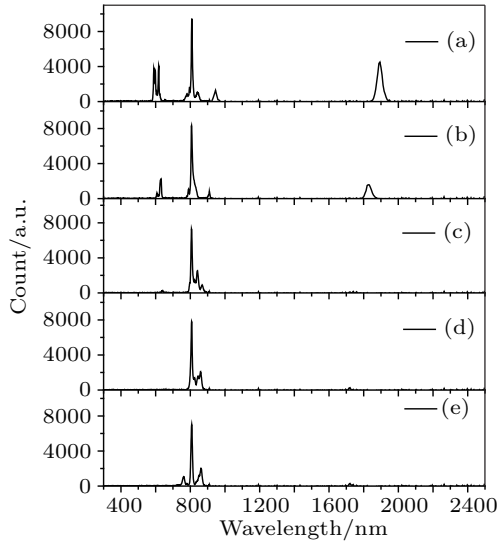


Fig. 4. Output spectrum of HB-MF with pump at 810 nm, pump power of 0.2 W. (a) 0°, (b) 30°, (c) 45°, (d) 60°, (e) 90°.

Figure 4 shows the output spectrum with Ti:sapphire laser pulse centered at 810 nm as pump. The average output power of Ti:sapphire laser is adjusted to 0.2 W and the input polarization angle θ is changed from 0° to 90°, where 0° means that the polarization direction of pump light is parallel to the slow axis of the HB-MF. When $\theta = 45°$, the output spectrum is barely broadened and the asymmetrical red-shift component mainly results from interplay of self-phase modulation (SPM) and simulated Raman scattering. There is no sign of Raman solitons, though the pump locates in the anomalous dispersion regime of both slow and fast axis. This can be explained by the fact that if two orthogonal modes are equally excited, the power distributed in each mode is too low to generate a Raman soliton. When θ is tuned to 30°, two modes have unequal amplitudes and the component along the slow axis dominates. Two fundamental solitons appear in the slow axis due to higher-order soliton splitting and red-shift to 1829 and 913 nm, respectively. During soliton self-frequency shift, dispersion wave (DW) with a central wavelength of about 630 nm is emitted. By adjusting the 1/2 wave plate to make the incident light polarize along the slow axis ($\theta = 0°$), two Raman solitons are further red-shifted to 1892 and 945 nm with blue shifting of DW because all the pump power is now coupled into x polarized mode. However, when the polarized direction of the pump light is tuned along the fast axis ($\theta = 90°$) to excite y polarized mode only, there is no sign of Raman solitons but two new sidebands, indicating the occurrence of modulation instability (MI). We attribute this to lower coupling efficiency of the pump and higher confinement loss along the fast axis, which makes the power coupled into the fast axis of HB-MF insufficient for Raman soliton generation. The deduction about the coupling efficiency and fiber loss can be verified indirectly by output power under different θ, obtained from numerical integral areas of output spectrum in Fig. 4. The output spectrum with $\theta = 60°$ is similar to that of $\theta = 45°$ because of the reasons mentioned above.

In Fig. 5, the red-shift of every fundamental soliton in each polarized axis increases with the pump power increasing from 0.3 to 0.5 W. When 810-nm incident pulse is tuned along either polarized axis of the HB-MF (see Figs. 5(a) and 5(b)), the furthest red-shift Raman solitons, which are most important in this paper, reach as far as 2030 and 2261 nm (MIR) with tunable bandwidth 178 nm and 277 nm for fast and slow axes, respectively. The strong output power of the furthest red-shift Raman solitons indicates that fiber loss is not the restriction factor to further red-shift of the solitons. In the experiment, searching for the red-shift limit of Raman solitons is hindered by the maximum output power of our Ti:sapphire laser. It is believed that a soliton redder than 2261 nm is achievable with higher pump power. The phase matched DW in the fast axis is a little more blue-shifted than that in the slow axis. This is the result of a smaller value of first λ_{ZDW} and larger value of dispersion in most of the anomalous dispersion regime of the fast axis than that of the slow axis, which is calculated and shown in Fig. 1. The condition when two orthogonal modes are equally excited ($\theta = 45°$) is also shown in Fig. 5(c) for comparison. The furthest red-shift Raman solitons of fast and slow axis still exist, while the red-shift extent is reduced to 1845 and 2038 nm due to lower soliton energy.

The pump wavelength's influence on the extent of SSFS is investigated in Fig. 6, while the output power of fs laser is set to be 0.5 W. For pump longer than 790 nm, the furthest red-shift Raman solitons can always reach MIR and the central wavelength of MIR solitons is monotonously increasing with the pump wavelength for both principal axes. However, it can be deduced that the second λ_{ZDW} at 2498 and 2110 nm of slow and fast axis will place restrictions on the red-shift limit of solitons. Beyond that wavelength, dispersion becomes normal and solitons cannot exist any longer. Compared with a soliton at the fast axis, the slow axis polarized soliton's red-shift velocity is much quicker, and only 20 nm change of pump results in 260 nm (from 2001 to 2261 nm) of MIR soliton tunability, which means a susceptibility to pump change but a wider tunable range.

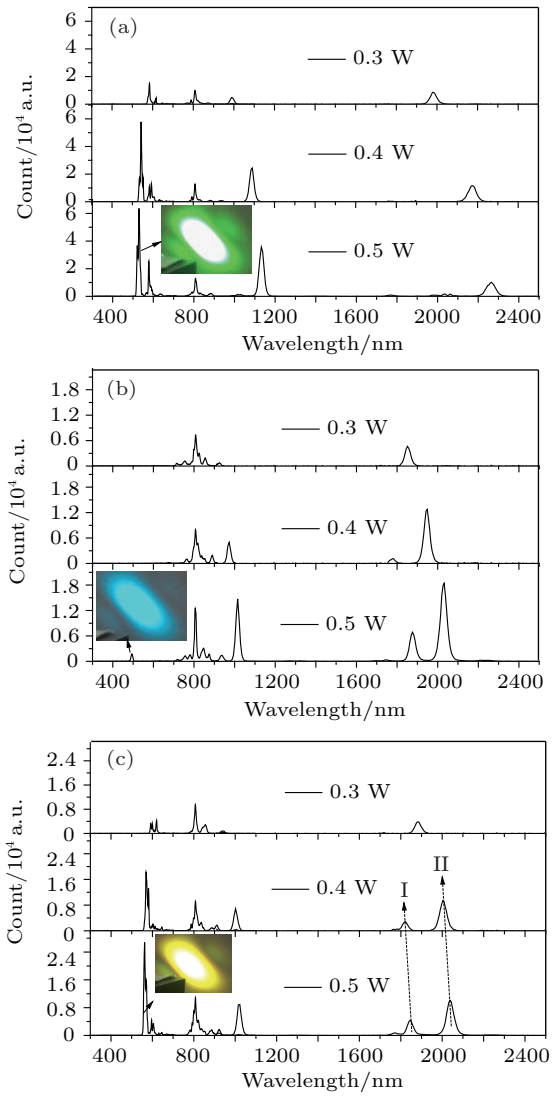


Fig. 5. (color online) Output spectrum with pump of 810 nm polarized along (a) slow axis, (b) fast axis, and (c) $\theta = 45°$ for different pump powers. In panel (c), peak I denotes the furthest red-shift Raman soliton in fast axis, and peak II denotes the furthest red-shift Raman soliton in slow axis.

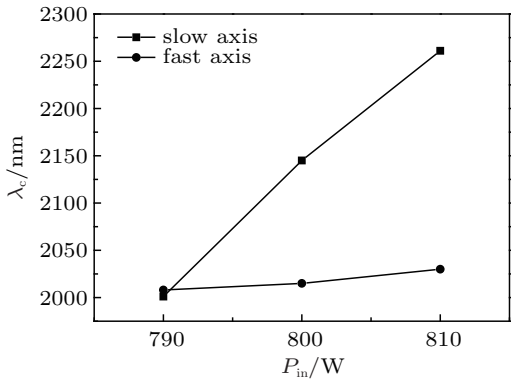


Fig. 6. Central wavelength λ_c of soliton as a function of the pump wavelength.

4. Conclusion

In summary, Raman soliton self-frequency shifted to mid-infrared ($\lambda > 2$ μm) has been achieved in an air-silica HB-MF by using Ti:sapphire fs laser as the pump. When the output wavelength of Ti:sapphire fs laser is tuned to 810 nm and the output power changes from 0.3 to 0.5 W, the furthest red-shift Raman solitons are shifted from near-infrared to mid-infrared, reaching as far as 2030 and 2261 nm for fast and slow axis, respectively. Raman soliton in mid-infrared can always be obtained for the pump with wavelength longer than 790 nm when output power of fs laser reaches 0.5 W. The strong output power of solitons indicates that fiber loss is not the primary reason to restrict the red-shift of Raman solitons, and higher pump power or longer pump wavelength would make the soliton red-shift further. However, the position of the second λ_{ZDW} of fast and slow axis polarized mode, which locates at 2110 and 2498 nm respectively, will decide the red-shift limit. Compared with the fast axis, the red-shift soliton in the slow axis has a wider tunable range: only 20 nm change of pump results in 260 nm (from 2001 to 2261 nm) of mid-infrared soliton tunability.

References

[1] Zlatanovic S, Park J S, Moro S, Boggio J M C, Divliansky I B, Alic N, Mookherjea S and Radic S 2010 *Nat. Photon.* **4** 561
[2] Nodop D, Jauregui C, Schimpf D, Limpert J and Tünnermann A 2009 *Opt. Lett.* **34** 3499
[3] Wei K H, Jing P P, Wu B, Chen T and Shen Y H 2015 *Chin. Phys. B* **24** 024217
[4] Chen Q J, Zhou G Y, Shi F K, Li D M, Yuan J H, Xia C M and Ge S 2015 *Acta Phys. Sin.* **64** 034215 (in Chinese)
[5] Dutta B and Helbing J 2015 *Opt. Express* **23** 16449
[6] Khlebtsov N G 2008 *Quant. Electron.* **38** 504
[7] Barghoorn P, Stebani U and Balsam M 1998 *Adv. Mater.* **10** 635
[8] Bennett P J, Monro T M and Richardson D J 1999 *Opt Lett.* **24** 1203
[9] Liu S and Li S G 2013 *Chin. Phys. B* **22** 074206
[10] Li D M, Zhou G Y, Xia C M, Wang C and Yuan J H 2014 *Chin. Phys. B* **23** 044209
[11] Brian W, Stephen R and Robert W 2002 *Opt. Express* **10** 575
[12] Kang Z, Yuan J H, Li S, Xie S L, Yan B B, Sang X Z and Yu C X 2013 *Chin. Phys. B* **22** 114211
[13] Washburn B R, Ralph S E, Lacourt P A, Dudley J M, Rhodes W T, Windeler R S and Coen S 2001 *Electron. Lett.* **37** 1510
[14] Liu X, Xu C, Knox W H, Chandalia J K, Eggleton B J, Kosinski S G and Windeler R S 2001 *Opt. Lett.* **26** 358
[15] Masip M E, Rieznik A A, König P G, Grosz D F, Bragas A V and Martinez O E 2009 *Opt. Lett.* **34** 842
[16] Cheng T L, Kanou Y, Asano K, Deng D H, Liao M S and Matsumoto M 2014 *Appl. Phys. Lett.* **104** 121911
[17] Ortigosa-Blanch A, Knight J C and Russell P S J 2002 *J. Opt. Soc. Am. B* **19** 2567
[18] Yu Y, Jia W G, Yan Q, Men K N and Zhang J P 2015 *Acta Phys. Sin.* **64** 054207 (in Chinese)
[19] Wang H C, Ling D X and He Y J 2015 *Chin. Phys. Lett.* **32** 074203
[20] Batian T 1985 *Appl. Opt.* **23** 4477